Suppression of the wake steady asymmetry of an Ahmed body by central base bleed

Tauha Irfan Khan and Vladimir Parezanović*
Khalifa University of Science and Technology, Abu Dhabi, UAE

Luc Pastur
ENSTA-Paris, Institut Polytechnique de Paris, Palaiseau, France

Olivier Cadot
School of Engineering, University of Liverpool, Liverpool L69 3GH, UK
(Dated: September 28, 2022)

Base Blowing is applied through a small, centrally-located square aperture at the base of a flat-backed Ahmed body. In addition to the expected drag reduction effect at low momentum injection (i.e. base bleeding effect), a major new result is the complete suppression of the steady asymmetry of the wake. Both the maximum drag reduction and the minimum magnitude of the base pressure gradient are achieved for the same optimal blowing coefficient of the actuator. Independent force measurements corroborate the suppression of the wake asymmetry. Different scales of base blowing reveal similar maximum drag reduction and asymmetry suppression, where the optimal blowing coefficient is found to scale with bleed-to-base area ratio as $(S_j/S)^{1/2}$.

The passive or active injection of fluid into the wake of a bluff body, commonly referred to as base bleed, is a well-known method of drag reduction. It has been widely used for both two-dimensional cylinders [1–3] and three-dimensional axisymmetric bodies [4–8]. More recently, base bleed has been examined in the case of square-back models as active base blowing [9–11], passive ventilation [12], and at industrial scales [13].

On the other hand, the turbulent wake of the flat-backed Ahmed body is dominated by the Reflectional Symmetry Breaking (RSB) mode [14] which causes the wake to switch chaotically between two stable, asymmetric states. This steady wake asymmetry, resulting from a pitchfork bifurcation [15], produces side forces and an increase in drag. The asymmetry can be mitigated by placing a small control cylinder in the wake, which can result in a drag reduction of around 4% [16, 17]. Thus, recent efforts have been directed towards the symmetrization of the wake, in order to remove the drag associated with the RSB mode. However, suppressing the RSB mode in the horizontal direction (y-instability) may lead to a permanent wake asymmetry in the vertical direction (z-instability) [10, 18–20].

The two cases in which the RSB mode has been completely suppressed in both directions use a rear cavity [21] and a perimetric base suction [22]. In the former case, drag has been reduced and base pressure fluctuations significantly damped, while in the latter base suction increased the overall drag, since the recirculation region shrinks due to mass extraction, but also achieved a symmetric wake in both vertical and horizontal directions. In the case of peripheral base blowing [10], the actuation has almost no authority on the steady asymmetry while low drag is observed. More recently, [23] used a large-scale Sweeping Jet actuator blowing from the middle of the Ahmed body base. They observed a significant reduction of the steady asymmetry in the wake, although not corresponding to a minimum drag. This result indicated that a centrally-located base blowing might be much more effective at symmetrizing the wake than blowing near the shear layers. Inspired by the latter work, we present the results on the drag reduction and suppression of the steady wake asymmetry by a steady jet blowing from the center of the flat-backed

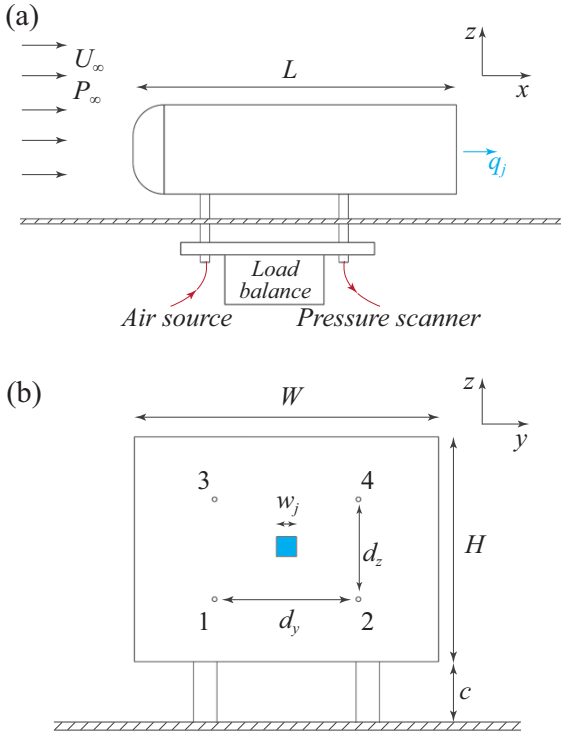

FIG. 1. Side (a) and rear (b) views of the experimental model.

* vladimir.parezanovic@ku.ac.ae

Ahmed body base. The effect of scaling for such type of base blowing is also presented.

The experiments were performed in an Eiffel-type wind tunnel with a test section of 390 × 400 × 1200 mm ($h \times w \times l$). The square-back bluff body, shown in Fig. 1, has dimensions of $H = 72$ mm, $W = 97.25$ mm and $L = 261$ mm. The model is mounted above the test section floor keeping a ground clearance of $c = 20$ mm. Four cylindrical support struts of 7.5 mm diameter are used to mount the model on a platform which is then attached to the load balance. These hollow struts provide access for the air supply for the actuator and the vinyl tubes between the pressure ports and the pressure scanner (which is located below the test section floor). The free stream velocity was maintained at $U_\infty = 13.5$ m/s which corresponds to a $Re = U_\infty H/\nu \approx 65,000$, where ν is the kinematic viscosity.

The actuation is performed by a centrally-located, steady jet at the base, as shown in Fig. 1. The jet is expelled through a simple square cross section duct of side (w_j), with the bleed-to-base area ratio of $S_j/S = w_j^2/HW = 0.0057$. The mass flow rate through the actuator is set using an ALICAT 2000 SLPM Flow Controller. The flow rate is represented by a dimensionless blowing coefficient $C_q = q_j/U_\infty HW$, where q_j is the volumetric flow rate supplied to the actuator.

Instantaneous pressure at the base of the bluff body $p_i(t)$ is measured through four static pressure ports, where $i \in 1, 2, 3, 4$ corresponds to labels in Fig. 1b. The ports are connected via flexible vinyl tubes to a Scanivalve ZOC 22B/32Px pressure scanner, and the pressure is acquired at a rate of 200 Hz over a period of $T = 30$ s. The instantaneous pressure is presented as a non-dimensional pressure coefficient $c_{p(i)} = (p_i(t) - P_\infty)/q_\infty$, where P_∞ and $q_\infty = \frac{1}{2}\rho U_\infty^2$ are the mean reference static and dynamic pressures of the test section obtained through a Pitot-static tube located upstream and away from the model. The contribution of the base to the pressure drag is expressed as a mean base suction coefficient, averaged over the four pressure ports:

$$C_B = -\frac{1}{4}\sum_{i=1}^{4} C_{p(i)}, \tag{1}$$

where $C_{p(i)} = \langle c_{p(i)} \rangle_T$ is the time-averaged value.

Instantaneous base pressure gradients in the horizontal and vertical direction are calculated as:

$$g_y = \frac{c_{p(4)} - c_{p(3)} + c_{p(2)} - c_{p(1)}}{2d_y/H} \tag{2}$$

and

$$g_z = \frac{c_{p(3)} - c_{p(1)} + c_{p(4)} - c_{p(2)}}{2d_z/H}, \tag{3}$$

respectively, where $d_y = 46$ mm and $d_z = 32$ mm are the separation distances between the pressure ports. The magnitude of the resulting pressure gradient is defined as $G = \left\langle \sqrt{g_y^2 + g_z^2} \right\rangle_T$ and represents the time-averaged strength of the wake asymmetry.

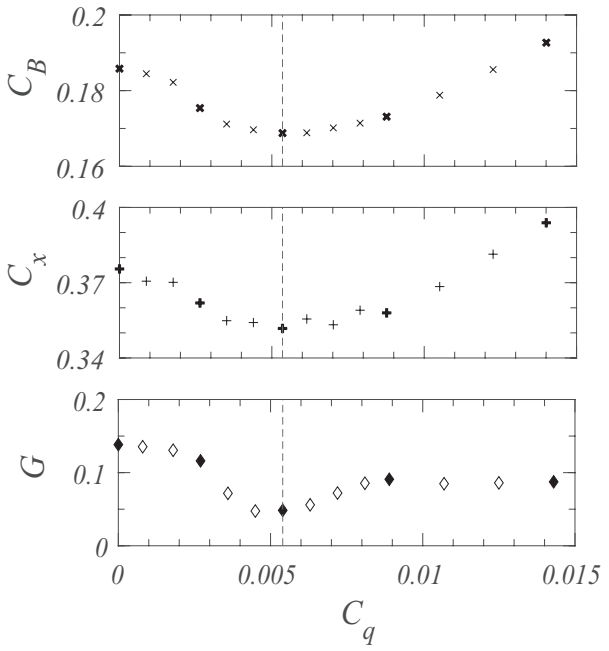

FIG. 2. Evolution of base suction (C_B), drag (C_x) and wake asymmetry strength (G) with respect to the blowing coefficient C_q. Dashed vertical lines correspond to C_q^{opt}. Highlighted points (filled markers) correspond to data points used in Fig 3.

Force measurements are performed simultaneously with pressure measurements, using a multi-axis load balance AMTI MC3A-500 at an acquisition rate of 1000 Hz and a period of $T = 30$ s. The measurements of forces are first performed with the model installed and wind tunnel switched off ($U_\infty = 0$), to characterize the contributions of actuation to the forces applied on the bluff body $f_{(q)k}$ ($k \in x, y, z$), for different C_q. The wind tunnel is then activated and, after a settling period, the measurements are obtained for the working velocity U_∞ and varying C_q. The instantaneous dimensionless force coefficients are then estimated as $c_k = (f_k - f_{(q)k})/(q_\infty HW)$, and the corresponding mean quantities are denoted as $C_k = \langle c_k \rangle_T$. Finally, the deviation of aerodynamic force coefficients with respect to C_q is defined as:

$$\Delta c_k = c_k(C_q) - C_k(C_q = 0), \tag{4}$$

where $c_k(C_q)$ is the instantaneous force coefficient for any given C_q, and $C_k(C_q = 0)$ is the mean force coefficient for the un-actuated flow.

Reference measurements for U_∞ and $C_q = 0$ are taken at the beginning and the end of each set of experiments, and are used to correct the pressure and force data for drift. According to the manufacturer specifications for the respective measurement systems, the precision of instantaneous pressure and force data in terms of dimensionless coefficients are $\delta(c_p) = \pm 0.04$, $\delta(c_x, c_y) = \pm 0.02$

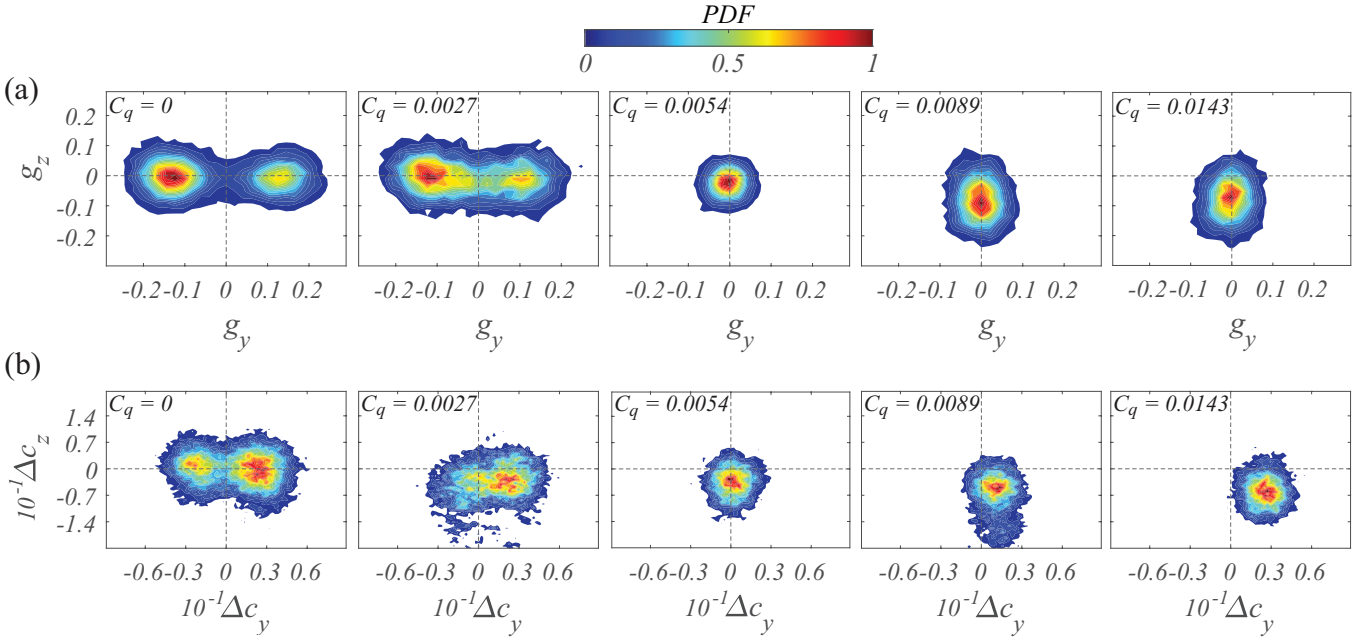

FIG. 3. The joint PDFs of (a) horizontal (g_y) and vertical (g_z) pressure gradients at the base, and (b) deviations of side force (Δc_y) and normal force (Δc_z) coefficients. Color bar represents normalized PDF with values below 0.004 as white.

and $\delta(c_z) = \pm 0.075$. However, the mean values of C_B and C_x satisfactorily converge after about 20 s of data, and the standard deviation of their averages over longer times (up to $T = 30$ s) are less than 0.11% and 0.24% of the mean values, respectively.

The global effects of base blowing for different C_q are encapsulated in Fig. 2. For the un-actuated flow, absolute values of base suction and drag coefficients are $C_{B0} = 0.185$ and $C_{x0} = 0.375$, respectively. The un-actuated values are comparable to data from a similar experiment in [10]. As blowing coefficient is increased, these values gradually decrease to a minimum at $C_q^{opt} = 0.0054$, where the base suction and drag coefficients are decreased by around 9% and 6%, respectively. For blowing coefficients $C_q > C_q^{opt}$ both quantities slowly increase and eventually show a net drag increase for $C_q > 0.012$. This behavior is observed also in the experiment of [10] and is discussed there in the context of the model of the recirculation region length by [24]. We hypothesize that in the current experiment the flow regime up to C_q^{opt} is similar to the "mass" regime, and beyond that value to the "momentum" regime, as proposed by [10]. However, the mass regime observed in [10] is characterised by an affine decrease of the drag until the minimum drag is reached. It is modelled by an affine increase of the recirculation length as a consequence of a passive mass injection (i.e.: where the momentum of the injected mass is negligible), thus changing globally the recirculating volume. Here, the behaviour observed in Fig. 2 becomes nonlinear much before the minimum drag is reached. One then suspects whether the interaction of the blowing jet with the feedback recirculating flow almost centered at the base contributes to extra drag reduction by for instance suppressing the RSB mode. As the injection in [10] is at the periphery of the base, it might miss this beneficial momentum effect. It can be observed that the slopes of C_B and C_x start to noticeably diverge from each other at high blowing rates ($C_q \gg C_q^{opt}$), which indicates that the base suction is no longer accurately estimated using the assumption of a uniform distribution of pressure at the base, due to the intense low-pressure region created by the blowing jet.

The strength of the steady asymmetry in the wake is also represented in Fig. 2, by the modulus of the base pressure gradient G. The high magnitude of G for $0 \leq C_q < 0.027$ indicates a strong asymmetry of the wake for un-actuated flow and low actuator mass flow rate cases. The modulus of the pressure gradient is significantly reduced at C_q^{opt}, coinciding with the strongest reductions of base suction and drag. At higher blowing coefficients, the wake asymmetry again starts to increase but does not achieve the levels of the un-actuated wake.

The presence of the wake RSB mode and its evolution, versus select C_q, are visualized by the Probability Density Function (PDF) of the pressure gradient $\mathbf{g}$ in Fig. 3a. The RSB mode in the horizontal direction is clearly visible for the baseline flow case ($C_q = 0$), where g_y can have a positive (P state) or a negative value (N state) with an almost equal probability. As the flow rate is increased to $C_q = 0.0027$, mode-switching between the two asymmetric flow states becomes more frequent, significantly populating the $g_y = 0$ bin, but high values of g_y are still highly probable. For $C_q^{opt} = 0.0054$ the pressure gradient reduces to a compact, circular distribution

centered around zero. This suggests the RSB mode has been suppressed in both horizontal and vertical directions. For higher C_q the vertical pressure gradient g_z adopts a steady N state, indicating that the wake has been vectorized downwards by the base blowing.

The changes to the wake RSB mode are corroborated by the PDF of the deviations of side force and lift force coefficients, in Fig. 3b. Almost identical patterns of PDFs between the pressure and the forces can be observed, up to and including C_q^{opt}. For $C_q \geq 0.0089$, the pressure indicates increased fluctuations around a weak N-state of g_z, which is reflected in the PDF of the lift force. However, the PDF of Δc_y indicates a progressive increase of the mean side force with the increase of C_q which is not observed by the pressure. Nevertheless, it is clear that at C_q^{opt} the fluctuating forces acting on the body are strongly suppressed and comparable in both horizontal and vertical directions. The force measurements confirm that the beneficial effects of the steady jet seen in the pressure gradient are not due to any unwanted interaction between the jet and the pressure measurements at the base, but that the wake is truly more steady and symmetric.

The effect of scaling for this type of flow actuation is also studied. Base blowing is carried out from a similar location using two scaled down actuators. In what follows, the baseline actuator is referred to as $\times 1$ whereas the scaled down actuators $\times 0.5$ and $\times 0.35$ represent scaling with respect to actuator side w_j. Fig. 4a shows the changes in base suction, defined as $\Delta C_B = C_B - C_{B0}$, for all scales of actuators. We observe that the scaled down actuators $\times 0.5$ and $\times 0.35$ achieve a similar base suction reduction as the $\times 1$ actuator, however the maximum drag reduction is achieved at a lower $C_q^{opt} = 0.0027$ and 0.0018 respectively. Result from experiment conducted by [11] is also shown as Lorite-B (maximum base suction reduction around 6%). It represents base blowing being carried out from a horizontal slit spanning the bottom edge of the base. It is observed that the present fluid injection mechanism appears to be more energy efficient compared to base blowing carried out near the shear layers, as greater drag reduction is achieved along with lower C_q^{opt}.

Following the same idea as in [11] that the transition between the mass and the momentum regimes defining C_q^{opt} occurs when the injected momentum flux reaches a maximum value Π from which the mass injection cannot be considered as a passive scalar:

$$\Pi = \rho_j u_j^{\text{opt}} S_j u_j^{\text{opt}} = \frac{\rho_j}{S_j} \left(q_j^{\text{opt}}\right)^2 . \tag{5}$$

Eq.(5) provides the scaling:

$$C_q^{\text{opt}} = b \sqrt{\frac{\rho}{\rho_j} \frac{S_j}{S}}, \tag{6}$$

where $b^2 = \Pi / \rho U^2 s$ is the dimensionless maximum momentum flux bared by the bubble consistent with the mass regime and ρ the density of the injected gas. In our case $\rho/\rho_j = 1$ and Fig. 4b confirms satisfactorily the scaling (6) with $b = 7.41 \times 10^{-2}$ for which all actuator scales collapse in the "mass" regime. The maximum injected momentum flux $b^2 = 5.49 \times 10^{-3}$ cannot be compared to that reported in [11] (6.4×10^{-5}). There, a dilution factor had to be introduced in (5) in order to reproduce

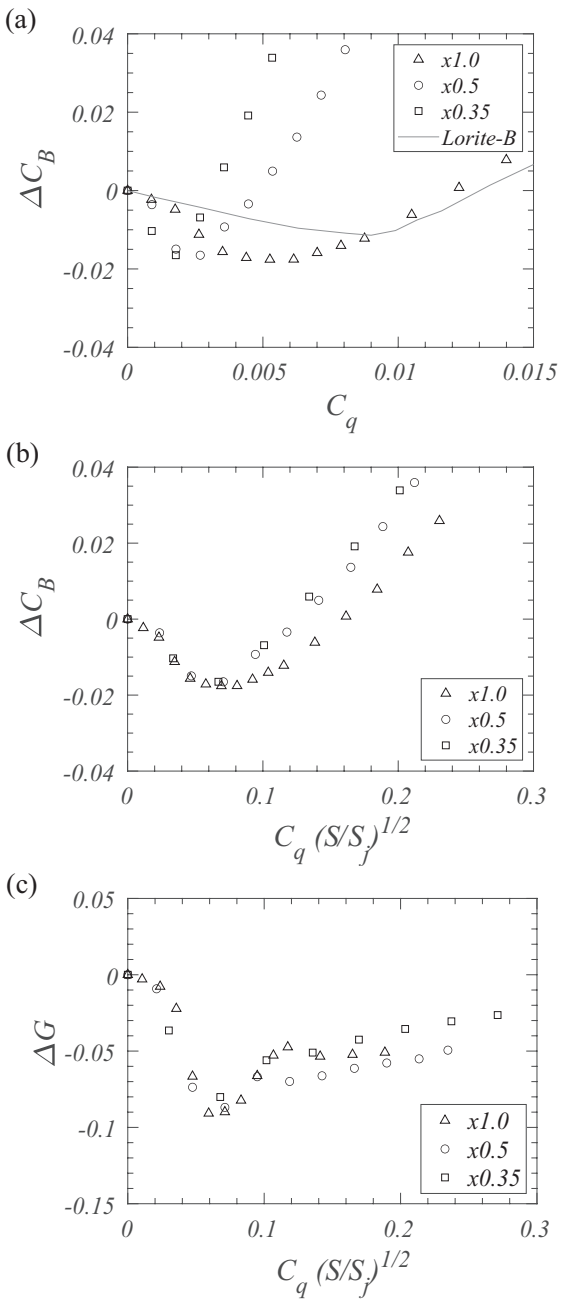

FIG. 4. Changes in base suction (ΔC_B) with respect to (a) the blowing coefficient C_q for all scales of steady jet actuator. Lorite-B results are from [11] (refer text), and (b) the scaled coefficient as power law of area ratio $C_q(S/S_j)^{1/2}$. (c) Changes in the wake asymmetry strength (ΔG) with respect to the scaled blowing coefficient $C_q(S/S_j)^{1/2}$ for all three scales of the actuation jet.

previous observation in [10] of a mass regime scaling with C_q, which is not the case here (see Fig. 4a).

The effects of the actuator jet scaling on the wake symmetry are shown in Fig. 4c with respect to the given scaling of the blowing coefficient. All three jet scales achieve a similar reduction in the wake asymmetry strength $\Delta G = G - G_0$. Furthermore, the $C_q(S/S_j)^{1/2}$ scaling reveal this to occur for the same actuation regime at C_q^{opt}.

To conclude, a centrally-located base blowing using a steady jet is found to greatly suppress the steady wake asymmetry, which otherwise dominates the un-actuated wake. A concurrent drag decrease of 6% is also recorded for the optimal blowing coefficient. A similar effect is also observed in the case of [23] and [25] when using a sweeping jet which is located centrally at the base, although the wake symmetrization does not correspond to a minimum drag, and the drag reduction is only around 3%. The square jet used in the current experiment has less entrainment and a lower spreading rate than a sweeping jet [26], and has no fixed frequency associated with it. These different dynamics plausibly account for the differences in the scaled blowing coefficients between the current experiment and results obtained by [25]. Furthermore, the scaling law coefficients differ from those observed in [11], indicating that both the blowing location and jet dynamics are the determining factors.

The proposed central blowing requires a lower mass flow rate of the actuator and provokes a greater drag reduction as compared to blowing from perimetric slits around the base [10, 11]. Recent studies by [27] suggest a feedback mechanism of recirculating flow from one shear layer interacting and triggering vortex rollups in the opposing shear layer that leads to wake reversal. They also identified that a transient symmetric state during wake reversals correspond to a lower base drag. On the other hand, in the experiments involving the base cavity [21] and base suction [22] where the wake is symmetrized, results cannot be easily interpreted in the context of the proposed mechanism by [27]. In both cases, there is no strong actuation which can plausibly inhibit the interaction of the opposite shear layers. In the example of our current work, the jet at C_q^{opt} is quite weak and it is doubtful (although not impossible) that it can act as an inhibitor of the proposed interaction mechanism. Extensive flow field data would be necessary to further study the underlying mechanisms.

ACKNOWLEDGMENTS

This work has been supported by the Khalifa University of Science and Technology under Award No. CIRA-2019-025. The authors would also like to thank T. Pichon and L. Cherfa of the ENSTA-UME, and R. De Jesus and R. Ganithi of the KU Fabrication Laboratory, for their exceptional support in this experiment.

[1] C. J. Wood, The effect of base bleed on a periodic wake, The Aeronautical Journal **68**, 477 (1964).
[2] P. W. Bearman, The effect of base bleed on the flow behind a two-dimensional model with a blunt trailing edge, Aeronautical Quarterly **18**, 207 (1967).
[3] V. L. Zhdanov, Effect of jet bleed out of the base of a model on the base pressure and frequency characteristics of wake flow, Journal of Engineering Physics and Thermophysics **71**, 627 (1998).
[4] J. L. F. Porteiro, C. E. G. Przirembel, and R. H. Page, Modification of subsonic wakes using boundary layer and base mass transfer, AIAA Journal **21**, 665 (1983).
[5] G. K. Suryanarayana and G. E. A. Meier, Effect of ventilation on the flowfield around a sphere, Experiments in Fluids **19**, 78 (1995).
[6] A. Sevilla and C. Martínez-Bazán, Vortex shedding in high reynolds number axisymmetric bluff-body wakes: Local linear instability and global bleed control, Physics of Fluids **16**, 3460 (2004).
[7] A. R. Oxlade, J. F. Morrison, A. Qubain, and G. Rigas, High-frequency forcing of a turbulent axisymmetric wake, Journal of Fluid Mechanics **770**, 305 (2015).
[8] J. M. G. de la Cruz, A. R. Oxlade, and J. F. Morrison, Passive control of base pressure on an axisymmetric blunt body using a perimetric slit, Physical Review Fluids **2**, 043905 (2017).
[9] R. P. Littlewood and M. A. Passmore, Aerodynamic drag reduction of a simplified squareback vehicle using steady blowing, Experiments in Fluids **53**, 519 (2012).
[10] M. Lorite-Díez, J. I. Jiménez-González, L. Pastur, C. Martínez-Bazán, and O. Cadot, Experimental analysis of the effect of local base blowing on three-dimensional wake modes, Journal of Fluid Mechanics **883**, 10.1017/jfm.2019.917 (2019).
[11] M. Lorite-Díez, J. Jiménez-González, L. Pastur, O. Cadot, and C. Martínez-Bazán, Drag reduction of three-dimensional bodies by base blowing with various gas densities, Physical Review E **102**, 10.1103/PhysRevE.102.011101 (2020).
[12] J. Howell, D. Sims-Williams, A. Sprot, F. Hamlin, and R. Dominy, Bluff body drag reduction with ventilated base cavities, SAE International Journal of Passenger Cars - Mechanical Systems **5**, 152 (2012).
[13] Y. I. Brown, S. Windsor, and A. Gaylard, The effect of base bleed and rear cavities on the drag of an SUV, in *SAE Technical Paper Series* (SAE International, 2010).
[14] M. Grandemange, M. Gohlke, and O. Cadot, Turbulent wake past a three-dimensional blunt body. part 1. global modes and bi-stability, Journal of Fluid Mechanics **722**, 51 (2013).
[15] O. Cadot, A. Evrard, and L. Pastur, Imperfect supercritical bifurcation in a three-dimensional turbulent wake, Physical Review E **91**, 063005 (2015).
[16] M. Grandemange, M. Gohlke, and O. Cadot, Turbulent wake past a three-dimensional blunt body. part 2. experimental sensitivity analysis, Journal of Fluid Mechanics **752**, 439 (2014).
[17] M. Grandemange, O. Cadot, A. Courbois, V. Herbert,

D. Ricot, T. Ruiz, and R. Vigneron, A study of wake effects on the drag of ahmed's squareback model at the industrial scale, Journal of Wind Engineering and Industrial Aerodynamics **145**, 282 (2015).

[18] D. Barros, J. Borée, O. Cadot, A. Spohn, and B. R. Noack, Forcing symmetry exchanges and flow reversals in turbulent wakes, Journal of Fluid Mechanics **829**, 10.1017/jfm.2017.590 (2017).

[19] Y. Haffner, T. Castelain, J. Borée, and A. Spohn, Manipulation of three-dimensional asymmetries of a turbulent wake for drag reduction, Journal of Fluid Mechanics **912**, 10.1017/jfm.2020.1133 (2021).

[20] D. Bao, J. Borée, Y. Haffner, and C. Sicot, Near wake interactions and drag increase regimes for a square-back bluff body, Journal of Fluid Mechanics **936**, 10.1017/jfm.2022.28 (2022).

[21] A. Evrard, O. Cadot, V. Herbert, D. Ricot, R. Vigneron, and J. Délery, Fluid force and symmetry breaking modes of a 3d bluff body with a base cavity, Journal of Fluids and Structures **61**, 99 (2016).

[22] E.-C. Hsu, L. Pastur, O. Cadot, and V. Parezanović, A fundamental link between steady asymmetry and separation length in the wake of a 3d square-back body, Experiments in Fluids **62**, 10.1007/s00348-021-03201-y (2021).

[23] D. Veerasamy, A. R. Tajik, L. Pastur, and V. Parezanović, Effect of base blowing by a large-scale fluidic oscillator on the bistable wake behind a flat-back ahmed body, Physics of Fluids **34**, 035115 (2022).

[24] J. H. Gerrard, The mechanics of the formation region of vortices behind bluff bodies, Journal of Fluid Mechanics **25**, 401 (1966).

[25] T. I. Khan, A. R. Tajik, and V. Parezanović, Drag reduction of a generic transport vehicle model using a fluidic oscillator, International Journal of Thermofluids **15**, 100180 (2022).

[26] F. Ostermann, R. Woszidlo, C. N. Nayeri, and C. O. Paschereit, Properties of a sweeping jet emitted from a fluidic oscillator, Journal of Fluid Mechanics **857**, 216 (2018).

[27] Y. Haffner, J. Borée, A. Spohn, and T. Castelain, Mechanics of bluff body drag reduction during transient near-wake reversals, Journal of Fluid Mechanics **894**, 10.1017/jfm.2020.275 (2020).